

# GPU-based Private Information Retrieval for On-Device Machine Learning Inference

Maximilian Lam  
Meta AI / Harvard University  
maxlam@g.harvard.edu

Jeff Johnson  
Meta AI  
jhj@meta.com

Wenjie Xiong  
Meta AI / Virginia Tech  
wenjiex@vt.edu

Kiwan Maeng  
Pennsylvania State University  
kwmaeng91@gmail.com

Udit Gupta  
Meta AI  
uditg@meta.com

Minsoo Rhu  
Meta AI / KAIST  
minsoo.rhu@gmail.com

Hsien-Hsin S. Lee  
Intel  
lee.sean@gmail.com

Vijay Janapa Reddi  
Harvard University  
vj@eecs.harvard.edu

Gu-Yeon Wei  
Harvard University  
guyeon@seas.harvard.edu

David Brooks  
Harvard University  
dbrooks@g.harvard.edu

Edward Suh  
Meta AI / Cornell University  
edsuh@meta.com

**Abstract**—On-device machine learning (ML) inference can enable the use of private user data on user devices without remote servers. However, a pure on-device solution to private ML inference is impractical for many applications that rely on embedding tables that are too large to be stored on-device. To overcome this barrier, we propose the use of private information retrieval (PIR) to efficiently and privately retrieve embeddings from servers without sharing any private information during on-device ML inference. As off-the-shelf PIR algorithms are usually too computationally intensive to directly use for latency-sensitive inference tasks, we 1) develop a novel algorithm for accelerating PIR on GPUs, and 2) co-design PIR with the downstream ML application to obtain further speedup. Our GPU acceleration strategy improves system throughput by more than  $20\times$  over an optimized CPU PIR implementation, and our co-design techniques obtain over  $5\times$  additional throughput improvement at fixed model quality. Together, on various on-device ML applications such as recommendation and language modeling, our system on a single V100 GPU can serve up to 100,000 queries per second—a  $> 100\times$  throughput improvement over a naively implemented system—while maintaining model accuracy, and limiting inference communication and response latency to within 300KB and  $< 100\text{ms}$  respectively.

## I. INTRODUCTION

Privacy is an important consideration for real-world machine learning (ML) applications as both regulations [6], [9] and corporate policies [3], [10] require more privacy protection of user data. For example, recent privacy policies for mobile platforms [3], [10] limit the type of user data that can be used for server-side computation [4]. Future ML services will need to increasingly rely on on-device compute to utilize most private user data.

On-device ML inference is a promising solution to stronger privacy regulations and policies [11], [39], [50], [76], as it enables model inference without requiring clients to share raw private input features with the service provider. Unfortunately, a completely on-device ML inference solution is impractical for many applications such as recommendation or language modeling, as these applications often require access to an

embedding table that is too large to store on device. For example, recommendation models access tables that often take gigabytes or even terabytes of memory [8], [40], [60], [61], [77]. Similarly, language models access word embeddings, which may take up to gigabytes of storage [23], [58], [63]. Large embedding tables pose a dilemma: storing large embedding tables on device is impractical given device limitations while storing them in the cloud and directly accessing them in the clear could leak private information.

To address this issue, we propose using private information retrieval (PIR) to privately query large embedding tables stored on centralized servers. In this work, we consider distributed point function (DPF)-based PIR, in which private embedding lookups are performed by constructing and evaluating DPFs on two non-colluding servers (Figures 1 and 3). A two-server DPF-PIR scheme is attractive as it is much more efficient in terms of computation and communication relative to other single-server PIR schemes [35], [56].

Despite their advantages, DPF-based PIR protocols still exhibit massive computational overhead [25], [36], making them difficult to deploy in real applications. The computational overhead stems from evaluating the DPFs on the servers, which entails executing a significant number of expensive cryptographic operations [25], [36]. For example, expanding a typical DPF for a table with one million entries requires performing at least one million AES-128 encryption operations. These costs are amplified during ML inference where a model may access multiple embedding entries simultaneously [40], [41]. The computation and communication requirements of DPF-based PIR make deploying it to real-world ML applications a considerable challenge.

### A. Our Contributions

In this work, we develop a system to efficiently and privately serve embeddings for on-device ML. Embedding accesses for on-device ML have several unique properties and requirements

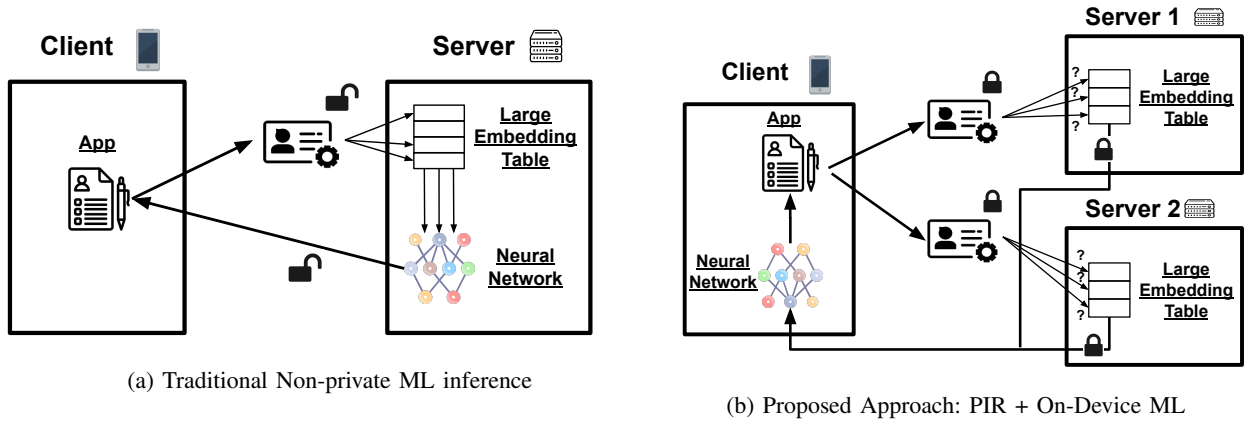


Fig. 1: Left: the traditional non-private approach to ML inference. Right: our proposed approach for private on-device ML inference. Our proposed approach stores large embedding tables on two non-colluding servers. Using PIR, a client privately obtains embeddings from the two servers which are subsequently used as inputs to their neural network.

relative to other applications that might use PIR: 1) embedding table entries are often short, on the order of 128-256 bytes, 2) multiple embedding table entries are often accessed together in a batch as part of a single model inference, and 3) throughput, latency, and model quality are all critical to an application's success. We leverage these properties to design a novel GPU acceleration scheme for efficiently performing PIR on GPUs, and, additionally, co-design PIR with the ML application to facilitate better trade-offs between model quality and system performance. Our technical contribution is similar in its nature to how recent studies co-optimize algorithms and GPU implementations to significantly improve the performance of other cryptographic primitives such as fully-homomorphic encryption (FHE) [28], [31], [34], [56]. Our key contributions are discussed in more detail below.

**GPU-accelerated PIR** We develop a set of novel optimizations to efficiently perform PIR on GPUs. Our optimizations enable high-throughput, low-latency DPF execution, allowing us to scale to tables with millions of entries. We observe that DPF evaluation is heavily compute-bound due to their heavy cryptographic instruction mix, and leverage the fact that GPUs are especially well suited to perform these computationally heavy operations. Yet, performing PIR on a GPU requires exploiting multiple types of parallelism in PIR while carefully balancing computation, communication, and memory usage. Our GPU acceleration, over an optimized CPU baseline [12], obtains  $> 1,000\times$  speedup over single-threaded CPU execution, and  $> 20\times$  speedup over multicore execution. To the best of our knowledge, this work represents the first to explore high-performance GPU implementations of DPFs. We note that our GPU implementation accelerates the state-of-the-art DPF algorithm [36], which exhibits an optimal communication cost of  $O(\log(n))$  and an optimal computation complexity of  $O(n)$ . Beyond private embedding table accesses for ML, our GPU PIR can be used to accelerate any PIR applications such as checking compromised passwords.

**ML + PIR Co-Design** To further improve performance, we develop strategies utilizing application-specific data access

patterns to co-design PIR with the ML application. Traditional batch PIR algorithms [18], [45], [48], which allow privately obtaining multiple entries together, may impact ML inference quality because they only retrieve entries probabilistically, dropping some queries spuriously. We co-design a new batch PIR algorithm for ML tasks to obtain better model quality vs system performance tradeoffs. We comprehensively evaluate the resulting performance improvements and model quality of our new batch PIR scheme on applications including Wiki-Text2 language model [57], MovieLens recommendation [43], and Taobao recommendation [15]. We find that by utilizing application-specific data access patterns, we can increase the ML inference throughput by up to  $100\times$  over a straightforward PIR system design on a multi-core CPU, while maintaining the model quality and limiting inference communication and latency within 300 KB and 100 ms, respectively.

## II. PRIVATE ON-DEVICE ML INFERENCE

### A. Private On-Device Inference: Threat Model

The goal of the private on-device inference is to perform ML inference using data on a user device without revealing them to a server owned by a service/cloud provider. We assume that the computation part of the ML model can run on the user device given the increasing trend on hardware accelerators and optimizations for client SoCs, but the *embedding tables* for categorical/sparse features (described below) are too large to be placed on individual devices. The embedding tables are still placed on servers and accessed remotely. In this model, the user/client device and its software are trusted while remote servers and communication channels are untrusted. Like other multi-party computation (MPC) settings [28], [31], [34], we consider a two-server model where there are two non-colluding servers; each server may try to obtain private user data from the embedding table accesses from the clients, but do not communicate/collude with the other. This work only considers the confidentiality of the user data and does not consider the integrity/correctness of the inference result. Figure 1 compares

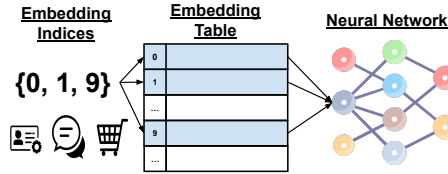


Fig. 2: Embedding tables map indices – numerical ids that represent information like user’s text messages or search history – into vectors of features that are inputs to a neural network model.

the traditional cloud-based ML services and the proposed on-device ML.

### B. Key Challenge: Large Embedding Tables

Unfortunately, the embedding tables that many ML models employ are too large to be sent and stored on individual devices [8], [40], [60], [61], [77], making a pure on-device inference solution impractical. An embedding table is a large table that maps categorical features into dense vectors that encode semantic information. For example, categorical (sparse) features may include a user’s click or search history. The value of a categorical feature is used as an index to an embedding table where each row of the table holds the vector corresponding to that categorical feature value (Figure 2).

Embedding tables have as many rows as the number of possible values in the categorical feature space so their size can grow quickly. For example, **recommendation models** use several user and product input features to predict whether a user is likely to interact (e.g., click or purchase) with the product [61], [77]. These models may use user data such as the list of products the user recently purchased [77]. As the number of products can be on the order of millions, the corresponding embedding table can reach several GB to TB in size [39], [40], [60]. Even though some systems may use a hash to reduce the size of an embedding table by sharing embedding table entries among multiple feature values, the embedding tables in real-world recommendation systems are still quite large. The large memory requirements of embedding tables prevent them from being stored on-device, and hosting them on the server may be the only practical solution.

Another example is **language models** that empower applications such as next-word prediction, language translation, and speech recognition. Language models map words into a latent embedding space using word embedding tables [57]. As there may be hundreds of thousands of different words, with each embedding vector being hundreds of bytes long, it quickly becomes impractical to store the entire word embedding table on-device, especially for natural language translation models supporting multiple languages [32], [62]. We emphasize that although there are alternative techniques to compresses these features (e.g., character embeddings, transformers, sentence level representations, etc.), word embeddings are more efficient to train in a regime with less training data [32]. Table I summarizes the size of the embedding tables of some popular

Application	# of Embedding Entries	Entry Size	Embedding Table Size
<b>Criteo 1 TB Recommendation</b>	>4,000,000,000	~128B	>476 GB
<b>Criteo Recommendation</b>	~45,000,000	~128B	~5 GB
<b>FastText Word Vectors (Language Model)</b>	~2,000,000	~1024B	>1.9 GB
<b>Taobao Recommendation</b>	~900,000	~128B	~109 MB
<b>WikiText2 (Language Model)</b>	~131,000	~512B	~64 MB
<b>Movielens-20M (Language Model)</b>	~27,000	~128B	~3 MB

TABLE I: Embedding table sizes for some popular datasets and models spanning across language and recommendation.

datasets/models, the size of which ranges from several MBs to hundreds of GBs.

### C. Our Approach: On-Device ML Inference with PIR

To enable private on-device ML applications that require access to large embedding tables, we propose using private information retrieval (PIR) [27], [31]. PIR allows a user to query a table without revealing which index was accessed to the table holder, i.e., the server that hosts the embedding table. We propose to keep large embedding tables on the application provider’s server, and to use PIR to query the table upon an embedding access by a client’s device (Figure 1).

We choose to use PIR rather than oblivious RAM (ORAM) [38], [69], [75], another popular cryptographic technique to hide an access pattern to memory, because ORAM is designed to protect accesses from a single entity. In order to use ORAM to hide accesses to embedding tables, the accesses from multiple user devices need to be serviced by a trusted ORAM controller, either a trusted proxy or secure hardware, while PIR allows private accesses from many individual user devices without such a trusted party. Additionally, recent work [31] shows PIR outperforms the state-of-the-art ORAM constructions, despite its  $O(n)$  asymptotic complexity. Alternatively, hardware-based protection such as a trusted execution environment (TEE) [2], [5], [13], [70] combined with ORAM [26], [33], [55], [64]–[66], [73], [74] may be used as a way to protect server-side accesses to embedding tables. However, the TEE-based approach places additional trust on hardware vendors and the security of today’s TEE protection mechanisms. Moreover, efficient hardware-based ORAM requires a custom hardware memory controller, which is not available today. Our PIR approach enables private embedding table accesses using today’s commercial off-the-shelf hardware like GPUs without needing to trust any hardware in the cloud.

Within the scope of PIR techniques, we use a PIR protocol based on a distributed point function (DPF) [25], [36], which protects accesses using two non-colluding servers. DPF-based PIR methods are more efficient in terms of communication and computation than single-server PIR schemes that employ homomorphic encryption [29], [35], [56]. A key challenge in employing DPF-based PIR is its high computational intensity

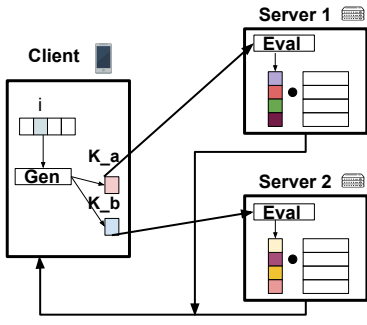


Fig. 3: DPF based PIR scheme.

due to their heavy cryptographic instruction mix. In the following section, we describe how the DPF-based PIR can be efficiently accelerated on GPUs.

### III. ACCELERATING PIR USING GPUS

Algorithms for PIR exhibit significant computational overhead due to their heavy cryptographic instruction mix and cannot be immediately adopted for private on-device inference. Below, we 1) briefly introduce PIR and DPF, 2) analyze their computational workload to understand how GPUs may accelerate them, and 3) describe our GPU acceleration algorithm.

#### A. Fundamentals of PIR and DPF

Private information retrieval (PIR) based on distributed point functions (DPF) allows a user to access an index in a table shared across two non-colluding servers without leaking the index to the table holders. In DPF-PIR, the client sends a key that represents the index it wants to privately query. The server, upon receiving the key, performs expensive cryptographic operations to service the user's query.

1) *Naive PIR*: Assume a client  $C$  seeks to privately access entry  $T[i] \in \mathbb{F}_p^D$  from a table  $T \in \mathbb{F}_p^{L \times D}$  that is duplicated across two non-colluding servers,  $S_1$  and  $S_2$ . Here,  $L$  is the number of entries in the table,  $D$  is the vector length of each entry, and  $\mathbb{F}_p$  is an integer field with modulus  $p$ . A simple but highly inefficient approach is for the client  $C$  to generate and send a random vector  $r_1 \in \mathbb{F}_p^L$  and a second vector  $r_2 \in \mathbb{F}_p^L$  to  $S_1$  and  $S_2$ , such that they add up to an indicator vector  $I(i)$  whose entries are all 0's except at the  $i^{th}$  position where it is 1 ( $r_1 + r_2 = I(i)$ ). Upon receiving the vectors, the servers individually compute and return  $T \times r_1$  and  $T \times r_2$  to the client, from which the client can retrieve  $T \times (r_1 + r_2) = T \times I(i) = T[i]$ . Information theoretic privacy is ensured as  $r_1$  and  $r_2$  are the *secret shares* of the indicator vector that do not leak any information about  $i$  individually [68]. This simple approach incurs large communication overhead because the size of  $r_1$  and  $r_2$  is proportional to the size of table  $T$ , making the communication overhead  $O(L)$ .

2) *DPF-PIR*: The generalization of the approach described above is a cryptographic primitive known as a **distributed point function** (DPF). Broadly, a DPF is an algorithmic construct that allows a client to **generate** two compact keys  $k_a, k_b$ , such that when the keys are **expanded** across a set of

indices, they yield secret shares of the indicator vector  $I(i)$ . Formally, a DPF consists of two algorithms

- $Gen(1^\lambda, i \in 1..L) \rightarrow (k_a, k_b)$  takes security parameter  $\lambda$  and input  $i$ , and generates two keys  $k_a, k_b$ .
- $Eval(k, j) \rightarrow \mathbb{F}_p$  takes a key  $k$  and an evaluation index  $j$  and outputs a field element.

such that,  $Eval(k_a, j) + Eval(k_b, j) = \begin{cases} 1 & j = i \\ 0 & j \neq i \end{cases}$ . A DPF

should be computationally secure, meaning that given just one of the keys and no other information, it should be difficult to recover  $i$  without doing computation proportional to  $O(2^\lambda)$ . Given a DPF, client  $C$  can generate keys  $k_a, k_b$  using  $Gen$  and send the keys to  $S_1$  and  $S_2$ , respectively. The two servers, upon receiving  $k_a$  and  $k_b$ , compute  $T \times Eval(k_a, \{0, 1, \dots, L\})$  and  $T \times Eval(k_b, \{0, 1, \dots, L\})$  and return the result, from which the client can obtain  $T \times (Eval(k_a, \{0, 1, \dots, L\}) + Eval(k_b, \{0, 1, \dots, L\})) = T \times I(i) = T[i]$ . Figure 3 depicts the overall DPF-PIR scheme.

There are many different implementations of DPFs, each with different computation/communication tradeoffs. We consider the DPF construct described in [36], which obtains optimal asymptotic communication complexity of  $O(\lambda \log(L))$  and optimal evaluation computation complexity of  $O(\lambda L)$ . The evaluation of DPF involves expanding a GGM-style [37] computation tree. Concretely, in this DPF algorithm, key  $k$  is decomposed into two codewords  $\{C_1 \in \mathbb{F}_{2^\lambda}^{2 \times \log(L)}, C_2 \in \mathbb{F}_{2^\lambda}^{2 \times \log(L)}\}$ , and the computation tree for DPF evaluation is specified by the following recurrence relation:

$$Eval(k, i) = Expand(k, i, d = \log(L))$$

$$= PRF_{Expand(k, \lfloor i/2 \rfloor, d-1)}(i \bmod 2) +$$

$$C_{Expand(k, \lfloor i/2 \rfloor, d-1) \bmod 2}[i \bmod 2, d]$$

where  $PRF$  is a pseudorandom function (i.e AES-128). Thus, computing  $Eval(k_a, \{0, 1, \dots, L\})$  involves evaluating each node of this computation tree (depicted in Figure 4). In terms of computation overhead, evaluating a single node requires a single  $PRF$  call and an addition, hence, the overall computation overhead of evaluating the entire set  $\{0, 1, \dots, L\}$  is  $O(\lambda L)$ . Communication overhead is proportional to the size of the keys, and, as these keys consist of codewords that are logarithmic in length, this amounts to  $O(\lambda \log(L))$  total communication. In practice,  $\lambda$  is typically a 128-bit field integer to ensure sufficient computational security. A figure depicting the DPF computation tree and its recurrence relation is shown in Figure 4. After computing the leaf nodes of the tree, the output is a vector of 128-bit field values; the final secret shares of the entry are obtained by performing an integer dot product between the computed 128-bit field values and the table. In practice, the dot products for multiple queries can be performed together as a single matrix-matrix multiplication. We refer to [36] for details on key generation.



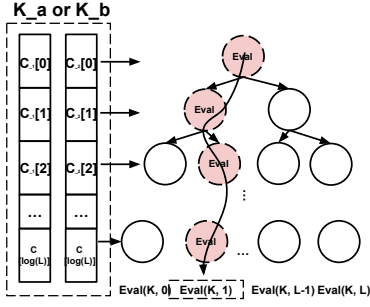


Fig. 4: Evaluating a distributed point function (DPF) involves expanding a binary computation tree all the way to the leaf nodes. The figure above displays the computation pattern of evaluating a DPF, where each node is a compute operation, and each edge represents a data dependency.

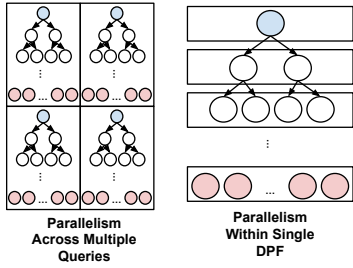


Fig. 5: Opportunities for parallelism. Left: multiple DPFs can be expanded simultaneously. Right: within a single DPF, each node at the same level may be computed simultaneously.

## B. Workload Analysis of DPF-PIR

DPF-PIR consists of two key computational operations: 1) expanding the DPF keys to obtain secret shares of the one-hot indicator vector and 2) performing a dot product between the vectors against the table of entries. These two operations exhibit significant compute parallelism that make them well suited for GPU execution. However, there are also significant challenges to parallelization. Below, we analyze the parallelism inherent in these workloads and the challenges associated with parallelizing them.

1) *Parallelism within a Single DPF*: Evaluating a single DPF involves the expansion of a balanced binary tree to its leaf nodes (Figure 4). The final leaf nodes represent secret shares of the final indicator vector that should be dot-producted with the table. As computing each node of the DPF evaluation tree relies only upon the completion of evaluating its parent node, we can parallelize the computation of the nodes provided that their parent node is already computed (Figure 5, right). Optimistically, each node at the same level of the DPF evaluation tree can be computed simultaneously, allowing  $2^i$  nodes to be derived in parallel at the  $i$ -th level. However, parallelizing a single DPF is not trivial, due to its tree computation structure. In particular, there is less parallelism near the root of the computation tree due, making smaller DPFs difficult to parallelize. Conversely, towards the leaf nodes of the tree, there is a significant number of nodes,

and computing them all simultaneously may run into memory limitation issues on larger tables.

2) *Parallelism across Multiple Queries*: A batch of DPFs may be expanded simultaneously by expanding multiple keys in a lockstep manner (Figure 5, left). Batching helps expose parallelism near the root of the computation tree where single-query parallelism is limited. However, batching also significantly increases memory usage near the leaves when caching the outputs of the nodes. Hence, It is important to ensure that execution maintains within the memory limitations, and to balance memory resources to ensure maximal parallelism.

3) *Computation and Memory Characteristics*: DPF-PIR consists of two main steps: the key expansion and the following dot product with the table. Both can be highly compute-bound, which makes GPU an ideal platform for acceleration. As seen in Figure 4, the size of a DPF key ( $k_a$  and  $k_b$ ) is  $O(\log(L))$  for a table of  $L$  entries, making the memory access of reading the key and writing the output  $O(\log(L)) + O(D)$ . In comparison, the computation needed to expand the key is  $O(L)$ , making the key expansion heavily compute-bound if  $D \ll L$ . For recommendation and language models,  $L$  can be up to 4 billion (Table I) while  $D$  is usually between 16 and 1024 (Table I), making DPF-PIR extremely compute intensive. While the dot product with the table is not necessarily compute-bound by itself, it can become compute-bound if we batch enough queries. We furthermore observe that the major bottleneck of the execution lies in the key expansion, due to its heavy cryptographic instruction mix. Finally, we note that DPF evaluation and matrix multiplication exhibit significantly different computational patterns, and naively performing one after the other leads to significant inefficiencies.

## C. Designing Efficient GPU Algorithm for DPF-PIR

This subsection describes our efficient GPU algorithm for accelerating DPF-PIR. Our base GPU algorithm leverages batched execution of multiple queries to a single table. The base algorithm is successively improved with a series of optimizations we propose that manage GPU memory limitations and balance memory and compute.

1) *Base Algorithm – Batch DPF Execution*: Our base approach leverages the fact that each DPF-PIR query to the same table can be expanded in an embarrassingly parallel fashion. We have each GPU thread-block handle expanding a separate DPF, with each thread of each thread-block expanding a different set of indices. Concretely, each thread of a thread-block individual computes a leaf node of the DPF evaluation tree, starting from the root node and traversing down to the leaf node. This base approach is shown in Figure 6a.

Although effective, the base approach has one key limitation: each thread-block expands the same node multiple times near the root, leading to significant redundant computations (Figure 6a, overlapped regions). This observation leads us to our first optimization.

2) *Optimization 1 – Eliminating Redundant Computations*: We optimize away the redundant computations near the root by introducing global memory buffers that cache and reuse the

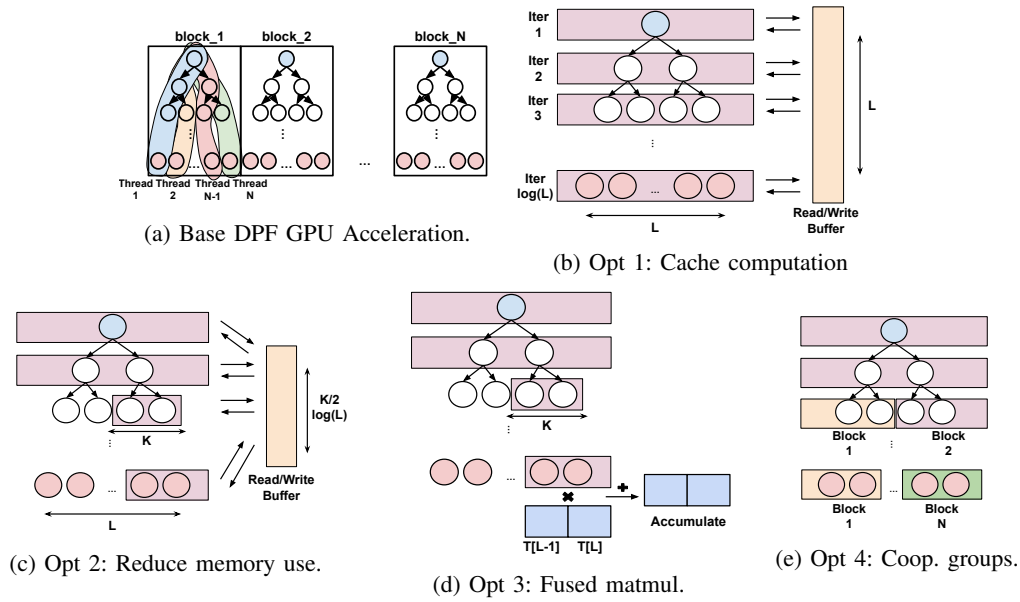


Fig. 6: Optimizations for accelerating DPF-PIR: a) parallelize DPFs across thread-blocks, b) eliminate redundant computation, c) reduce memory use, d) interleave matmul and DPF evaluation, e) parallelize with cooperative groups for large evaluations.

the output of the previous level of the tree, and synchronize the thread-blocks across levels (Figure 6b). Our optimization operates in a breadth-first manner, where each thread of a thread-block evaluates a different node for each level of the tree, and writes the result to a global memory buffer for the next level to use without recomputation. Synchronization barriers are inserted between levels for coordination.

While this optimization significantly improves over base-line, it requires a large global memory buffer of size  $O(BL)$ , where  $L$  is the number of table entries (i.e., number of nodes) and  $B$  is the batch size. As  $L$  may be large for certain applications,  $B$  can be limited. Hence, on large tables parallelism is limited. The next optimization tackles this problem.

3) *Optimization 2 – Optimizing Memory Usage:* To limit memory usage but enable efficient parallel execution of workloads, we switch to a hybrid breadth-first and depth-first evaluation strategy. Instead of expanding *all* the nodes in each level in a fully breadth-first manner, we expand only  $K$  nodes at a time in a depth-first fashion (Figure 6c). In this approach, the global memory buffer acts like a stack, where each depth-first traversal down the tree pushes  $K/2$  extra nodes to the stack. The memory overhead is reduced to  $O(BK \log(L)/2)$  instead of  $O(BL)$ , as the size of the stack grows by  $K/2$  nodes each level down, and there are  $\log(L)$  levels in the tree. The expansion factor  $K$  is empirically selected to expose enough parallelism while remaining within memory constraints.

4) *Optimization 3 – Matrix Multiplication Fusion:* We observe that the DPF and the subsequent matrix multiplication can be fused together for additional performance improvement. Upon reaching the leaf nodes, instead of writing the output to a buffer to later be used for the subsequent matrix multiplication, we can immediately compute a dot product between the partial output and the corresponding table entry for that index (Figure

6d). We accumulate these partial results in a thread-local register, and run a parallel tree-sum reduction at the end to obtain the final result. Fusing the DPF with the following matrix multiplication allows us to reduce memory usage and interleave compute and memory operations, overall leading to higher performance.

5) *Optimization 4 – Cooperative Groups for Very Large Tables:* We also leveraging cooperative groups [14] to accelerate DPF-PIR for very large tables (Figure 6e). On very large tables (e.g., with 4 million entries), there is sufficient parallelism to fully utilize the GPU, and batching multiple queries yields little performance benefits, and may in fact degrade latency. Hence, for very large tables, we employ cooperative groups [14] to coordinate all thread-blocks towards evaluating a single DPF tree. This technique obtains benefits when the table is very large, which may be the case in large recommendation systems [61], [77].

6) *Optimization 5 – PRF Selection:* Finally, we explore different pseudorandom functions (PRFs) to improve computational efficiency on a GPU. Standard implementations of DPF-PIR on CPUs utilize AES-128 [52]. However, unlike CPUs, GPUs lack hardware intrinsics that accelerate AES operations and hence may experience degraded latency and throughput. Thus, we explore different PRFs, including SHA-256 [42], Salsa20 [22], HighwayHash [17], and Siphash [20]. Among these, we observe that Salsa20 with 20 rounds (Salsa20-20) provides a good balance between high performance and strong security (it is a variant of a standard cryptographic stream cipher used in TLS [7]), which we use as our default PRF. However, other methods like Salsa20 with 12 rounds (Salsa20-12) or HighwayHash have better performance, potentially with lesser security guarantees. Depending on the use case, these alternative PRFs may be selected for better performance.

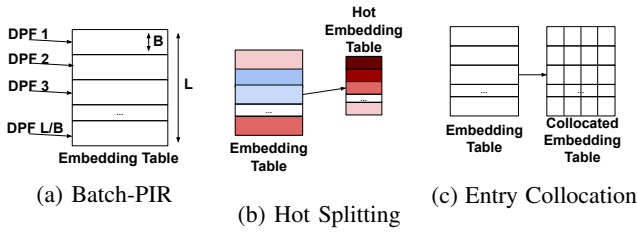


Fig. 7: Techniques used to co-design PIR + ML. a) Partial Batch Retrieval, b) splitting the table into a smaller hot table, and c) collocating frequently accessed entries.

#### IV. ACCELERATING BATCH RETRIEVAL WITH ML CO-DESIGN

In many recommendation/language models, each inference requires multiple lookups to the same embedding table. For example, recommendation models may lookup the same table hundreds of times to perform a single inference [40] (e.g., a user can have multiple clicked items, if the clicked-item history is used as a feature). Multiple lookups increase costs linearly as DPFE-PIR only retrieves one entry at a time.

To accelerate multiple lookups to a single table, we adopt partial batch retrieval (PBR) [67], an algorithm that accelerates the retrieval of multiple entries. PBR comes at a cost; with some probability, queries are spuriously dropped, which may negatively affect model quality. Additionally, naively adopting PBR is still quite computationally expensive. Hence, we co-design PBR with ML inference to improve system performance while maintaining the model quality.

##### A. Background: Batch Private Information Retrieval

Batch private information retrieval (batch-PIR) is a set of techniques to retrieve multiple private entries from a single table. In this work, we adopt the method proposed in [67], partial batch retrieval (PBR), which operates by segmenting table  $T$  into  $\frac{L}{B}$  bins of size  $B$ , and issuing individual DPFE-PIR queries to each bin (Figure 7a). This approach saves computation by a factor of  $\frac{L}{B}$  in the best-case scenario where the client retrieve  $\frac{L}{B}$  entries that are spread across each bin. PBR, unlike other batch-PIR methods, relies

However, there is a complex tradeoff space between the communication efficiency and the accuracy of the retrieval. A large  $B$  can reduce the accuracy of the retrieval if multiple desired entries fall in the same bin. Conversely, a smaller  $B$  yields fewer conflicts, but increases communication costs. This tradeoff naturally affects model quality as dropped queries affect the model’s inference.

##### B. Co-Designing the ML Model and Batch-PIR

To improve batch-PIR efficiency while minimizing effect of retrieval failures, we propose several co-designs that improve the tradeoff between model accuracy and performance.

1) *Frequency-Based Hot Table Split*: Many ML applications access embedding tables following a power-law distribution, where a small number of *hot* indices account for the majority of lookups [16], [41]. We leverage this observation

and add a small *hot table* that holds the top- $K$  frequently accessed indices in addition to the large *full table* that holds all the embedding entries (Figure 7b). The hot table is constructed statically using the observed statistics from the training dataset, and a small hash table is placed on a client device to provide the hot table index for the categorical feature values that are in the hot table.

However, simply using the hot table as a traditional cache is insecure as it leaks the number of queries to the hot/full tables. To avoid this information leakage, we predetermine a fixed number of queries  $Q_{hot}$  and  $Q_{full}$  to issue to the hot and full tables, respectively. The hot table leverages the fact that indices that are queried frequently can be stored all in the compact table; multiple queries issued to the hot table benefit from the lower PIR costs from the reduced table size. Because  $K$ ,  $Q_{hot}$ , and  $Q_{full}$  are all fixed at design time, each inference does not leak additional information about the client.

2) *Access Pattern-Aware Embedding Collocation*: Embedding table access patterns in ML applications tend to exhibit co-occurrence [30], [54]; certain indices are often accessed together in a single ML inference. This property allows us to collocate frequently accessed entries in the same row of the table, so that a single query can retrieve multiple embeddings that might be accessed together (Figure 7c). Collocation can be done by profiling the training dataset and collocating the top- $C$  embeddings that are most frequently retrieved with each embeddings.  $C$  is empirically selected. In the best-case scenario, collocation can reduce the number of queries by  $C + 1$ . Collocation increases computation and communication costs as larger rows are retrieved for each query. However, with the right hyperparameters, this cost may be outweighed by the increase in query hits from the additionally retrieved entries. Note that the cost of DPFE computation for most tree nodes except for the leaves is independent of the size of an embedding table entry. As a result, the co-location only increases the cost at the leaves.

#### V. EVALUATION

##### A. Evaluation Setup

We evaluate our GPU-based DPFE-PIR and compare it with a state-of-the-art CPU implementation [12]. We run all GPU experiments on a NVIDIA V100 GPU, and all CPU experiments on an Intel(R) Xeon(R) Gold 6230 CPU @ 2.10GHz with 28 cores. The CPU baseline is an optimized DPFE-PIR implementation from Google Research [12], which uses AES-NI CPU hardware acceleration. Unless otherwise specified, We default to a security parameter of  $\lambda = 128$  bits, with each table entry containing 256 bytes.

For the machine learning evaluation, we use public datasets for language and recommendation models. For the language model, we train an LSTM on the Wikitext2 corpus [57]; the embedding table has 131,000 entries (Table I). For the Movielens [43] recommendation, we train a 2-layer neural network; the embedding table for the Movielens dataset has 27,000 entries. For the Taobao recommendation [15], we train a 2 layer fully-connected model combining both user

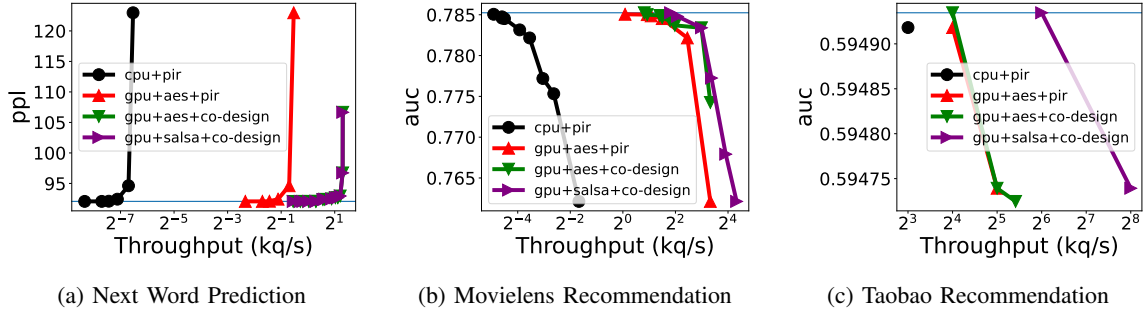


Fig. 8: Gains of GPU-DPF + co-design over a CPU implementation without PIR+ML co-design. Latency fixed to be  $< 200\text{ms}$  and communication  $< 500\text{KB}$ . Baseline model quality is shown in teal. For next word prediction, lower perplexity (ppl) is better; for recommendation models, higher area under curve (auc) is better.  $1 \text{ kq/s} = 1,000 \text{ queries per second}$ .

Application	Method	Model Quality	Communication (KB)	PIR Latency (ms)	Throughput (queries/s)	Throughput Speedup
Language Model	CPU+PIR	92 ppl	239	62	5.7	<b>200x</b>
	GPU+Co-design	92 ppl	425	8	<b>1,230</b>	
Movielens Recommendation	CPU+PIR	.785 auc	154	30.6	44	<b>95x</b>
	GPU+Co-design	.785 auc	52	82.4	<b>4,200</b>	
Taobao Recommendation	CPU+PIR	.595 auc	2.8	160	8,000	<b>32x</b>
	GPU+Co-design	.595 auc	5.4	150	<b>256,000</b>	

TABLE II: Representative ML inference performance points for CPU PIR vs our system with GPU accelerated PIR and ML co-design. Inference latency and communication are fixed to be  $< 200 \text{ ms}$  and  $< 300 \text{ KB}$  respectively, while maximizing throughput.

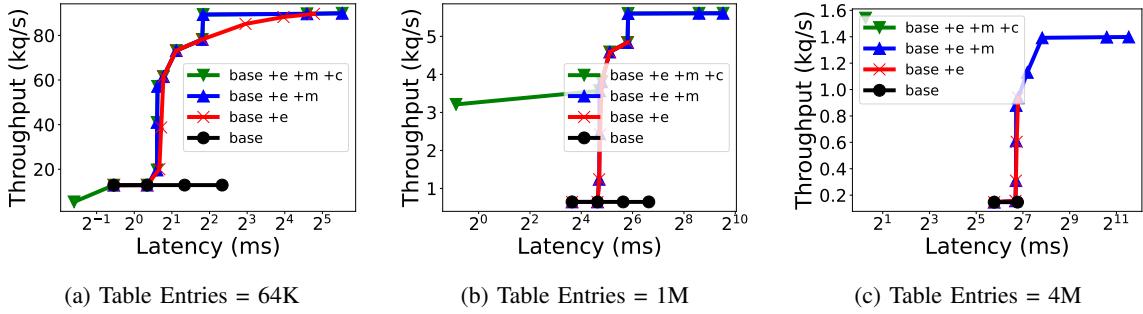


Fig. 9: Throughput vs latency for our GPU acceleration strategy across different optimizations and table sizes. Our optimizations include eliminating redundancy, memory optimization, cooperative groups.  $1 \text{ kq/s} = 1,000 \text{ queries per second}$ .

Table Size	Upload Communication (Bytes)	Strategy	Throughput (queries / s)	Latency (ms)
16K	896	GPU	60,347	3.2
		CPU 1-thread	22	9
		CPU 32-thread	281	.71
64K	1024	GPU	15,258	18.5
		CPU 1-thread	5	36
		CPU 32-thread	688	2.9
1M	1280	GPU	1358	1.4
		CPU 1-thread	1.3	638
		CPU 32-thread	21.2	36
4M	1408	GPU	468	4.18
		CPU 1-thread	.78	2579.8
		CPU 32-thread	12	160.1

TABLE III: Throughput / latency comparison of our GPU acceleration algorithm vs single and multi-core CPU implementations. Both use AES-128 as their PRF, and a security parameter of 128. The CPU DPF baseline is taken from [12] and is an optimized CPU implementation that uses AES-NI hardware intrinsics.

click-history and user features; the embedding table for Taobao has  $\sim 900,000$  entries (Table I).



Table Size	Throughput (queries/s) No Fusion	Latency (ms) No Fusion	Throughput (queries/s) With Fusion	Latency (ms) With Fusion	Throughput Improvement	Latency Improvement
16K	193000	1.49	348000	.9	1.8 $\times$	1.6 $\times$
64K	49000	5.8	89000	3.55	1.8 $\times$	1.6 $\times$
1M	2898	92	5578	56.5	1.9 $\times$	1.6 $\times$
4M	759	369	1395	226	1.8 $\times$	1.6 $\times$

TABLE IV: Impact of fusing and interleaving DPF expansion with matrix multiplication kernels, across different table sizes. Each entry in the table is 256 bytes.

### B. End-to-End System Performance Speedups

We begin by showing the final system throughput improvement of combining GPU acceleration with co-design over using state-of-the-art CPU-based PIR for ML inference. Figure 8 shows the system performance numbers across different applications. In Figure 8, we fix a latency budget of  $< 100$  ms and a communication budget of  $< 300$  KB per inference. As seen, accelerating PIR with GPU and co-designing it with ML inference leads to significant throughput improvement at the same accuracy. We highlight some of the representative datapoints in a tabular format in Table II. Accelerating PIR with GPUs and co-designing PIR with ML obtains up to over  $100\times$  increase in throughput at the same model quality.

### C. Detailed Analysis of Each Optimization

Below, we evaluate each of the optimizations separately to show the isolated effects of each optimization we propose.

1) *Effects of Each GPU Optimization:* Figure 9 shows an ablation of the throughput and the latency of our GPU-DPF acceleration with each successive optimization. As shown, each successive optimization increases the latency-throughput pareto frontier. Particularly, on smaller table sizes ( $< 64K$  entries, Figure 9a), we see that the base approach along with eliminating redundancy (**base+e**, red) is generally able to obtain fairly good performance, achieving  $4\text{--}5\times$  throughput improvement over the baseline (**base**, black). However, on larger table sizes ( $> 64K$  entries, Figure 9b– 9c) **base+e** is unable to improve the throughput after some point (disconnected red line around  $2^6$ ms) as memory constraints limit the batch size. On these larger tables, our memory optimization (**base+e+m**, blue) provides a far better latency-throughput tradeoff. Finally, for extremely large table sizes ( $> 4M$  entries, Figure 9c), cooperative groups is able to obtain significantly better latency (**base+e+m+c**, green). We additionally highlight some of these representative performance points in Table III

2) *Performance Impact of Matrix Multiplication Fusion:* Table IV shows the performance benefits of fusing the subsequent matrix multiplication with the DPF expansion on the memory-efficient GPU-PIR acceleration strategy, across different table sizes. Generally, fusing and interleaving the two kernels offer significant ( $> 1.5\times$ ) speedups in throughput and latency as it allows more efficient scheduling of compute and memory operations.

3) *Performance Impact of Embedding Entry Size:* We evaluate the impact of varying the size of the table entries on PIR performance. Recall that the size of the table entries affects the amount of work done in the subsequent matrix multiplication, and hence may affect throughput and latency. We show the

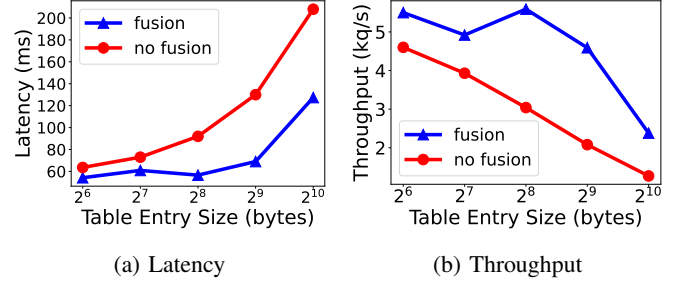


Fig. 10: Performance impact of table entry size on PIR performance, for a table size of 1,048,576.

impact of table entry size on latency and throughput in Figure 10. Generally, we find that we can retrieve tables that have entry sizes of up to 512 bytes with little to no performance degradation. This effect is helped significantly by fusing the DPF/matrix multiplication, as this allows us to interleave the memory operations required for the matrix multiplication along with PRF evaluations. We see increasing performance degradation with table entry sizes greater than 512 bytes. The minimal performance impact up to 512 bytes also illustrates the opportunity for the proposed co-location optimization.

4) *Comparison against CPU:* We compare our GPU-PIR implementation against an optimized CPU implementation from Google Research [12]. Note that, Google Research’s CPU implementation of DPFs uses AES-128 for its PRF, and utilizes AES-NI hardware intrinsics to accelerate PRF computation. Figure 11 compares the throughput attained by the memory-efficient GPU DPF acceleration strategy against a 1-threaded and 32-threaded CPU version, on different table sizes. Generally, using AES-128 as the PRF, our GPU implementation consistently attains  $> 17\times$  speedup over the 32-threaded CPU implementation, which fully utilizes the entire multi-core CPU. With a different choice of PRF, in this case Salsa20 with 12 rounds, we see over  $100\times$  speedup over multithreaded CPU execution. We show the same data in Table III. Generally, our GPU-based PIR can accelerate PIR by more than an order of magnitude over the CPU.

5) *PRF Evaluation:* We evaluate the performance impact of using different functions for the PRF when computing the DPF. Table V shows the results on a table of size 1M, using the memory-efficient DPF acceleration strategy, with a batch size of 512, and a security parameter of 128-bits. Generally, we find that lightweight PRFs can significantly improve the GPU-PIR performance over AES-128. For example, the Salsa20 stream ciphers with different numbers of rounds provide good performance while appropriate security. While Salsa20 with

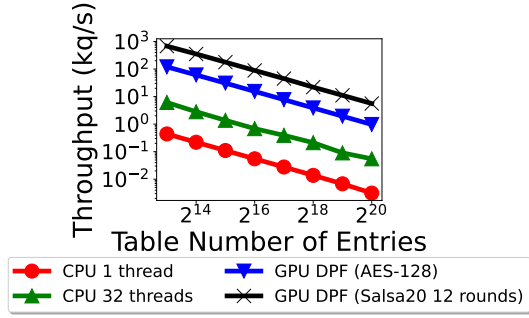


Fig. 11: Comparison of throughput performance attained by GPU DPF acceleration against an optimized CPU baseline. 1 kq/s = 1,000 queries per second.

PRF	Function Type	Latency (ms)	Throughput (queries/s)
AES-128	Block Cipher (Ctr Mode)	591	965
Salsa20-20	Stream Cipher	174	3640
Salsa20-12	Stream Cipher	113	5598
SHA-256	Hash (HMAC)	659	921
SipHash	PRF	82.3	7447
HighwayHash	PRF	320	1973

TABLE V: Performance evaluation of memory-efficient GPU DPF with different PRF functions, on a table of size 1,048,576, with batch size 512, and a security parameter of 128 bits.

8 rounds has been broken [21], Salsa20 with 12 and 20 rounds has no known attack. In particular, we believe that Salsa20 with 20 rounds will be a good choice as its variant, ChaCha20, is used as a standard in TLS. Thus, choice of PRF has significant performance implications and must be chosen depending on the security and performance requirements of the target application.

#### D. PIR + ML Co-Design

Private on-device ML inference often requires the private retrieval of a batch of embeddings from the same table. We evaluate our techniques that co-design ML inference and batch PIR, and demonstrate how our co-design techniques significantly improve model quality vs system performance tradeoffs.

1) *Computation vs Model Quality*: We show the tradeoff between computation and model quality given a fixed communication limit. Figure 12 shows this tradeoff across various applications when communication is fixed to be less than 300KB. As shown, the co-design with both a hot table and embedding entry collocation obtains up to 2–3 $\times$  improvement in computation at a fixed model quality.

2) *Communication vs Model Quality*: We show the tradeoff between communication and model quality given a fixed computation limit. Figure 13 shows this tradeoff across various applications, with computation fixed to be less than 100,000 PRF calls per batched inference (with the exception of Taobao, where the computation limit is fixed to be less than 5,000,000

PRF calls per batched inference). Again, co-designing PIR with the ML model obtains up to 2–4 $\times$  improvement in communication at a fixed model quality.

3) *Communication vs Computation*: We show the tradeoff between computation and communication with the fixed model quality. Figure 14 shows this tradeoff across various applications, with model quality fixed to be within 2% of the full precision baseline. The co-design optimizations obtain significantly better tradeoffs than plain batch-PIR.

4) *End-to-End Performance vs Model Quality*: Finally, we show the end-to-end throughput vs model quality across different applications, with communication fixed to be below 300KB and latency fixed to be below 100ms. Figure 15 shows the benefits of co-design on final throughput vs model accuracy, and demonstrates up to 2.5–4 $\times$  performance improvement.

## VI. RELATED WORK

**Privacy-preserving Computation Techniques** The previous work on privacy-preserving ML investigated running ML models on an untrusted cloud using various secure computing techniques such as FHE [49], [59], MPC [51], [53], [72], and trusted execution environments (TEEs) [46], [47]. Yet, these studies mainly focused on protection computation in convolutional neural networks (CNNs) without embedding tables. This work investigates how we can address privately accessing large embedding tables in recommendation and language models through PIR. ORAM [33], [38], [66], [69] with a TEE or a trusted third-party will be another way to protect embedding table accesses on an untrusted cloud. Here, we use PIR in order to allow accesses from many client devices without any secure hardware or trusted third-party.

**Private Information Retrieval** PIR can be broadly categorized into single-server protocols based on homomorphic encryption [29], [35], [56] and two-server protocols based on DPFs. We use a two-server PIR protocol for its efficiency. The two-server PIR protocols may run by using two different cloud providers or forming a consortium of multiple companies that need to provide privacy-preserving ML services to their users. Distributed point functions [24], [25], [36] are commonly used for efficient two-server PIR. An early PDF algorithm [24] demonstrated  $O(\sqrt{n})$  communication complexity and  $O(n)$  computation complexity. More recent advancements [25], [36] reduce the communication and computation costs to  $O(\log(n))$  and  $O(n)$ , respectively. A major contribution of our work is the efficient implementation of the  $O(\log(n))$  DPF algorithm on a GPU. To our knowledge, this work represents the first thorough study of efficiently parallelizing DPFs on GPUs. Parallelization DPFs on GPUs significantly improves the state-of-the-art for the DPF performance and makes DPFs far more practical in real-world use cases.

**Batch Private Information Retrieval** Various approaches for batch PIR [18], [19], [45], [48], [67] have been proposed. These methods typically use a form of bucketing and hashing to reduce storage costs. Our work utilizes partial batch retrieval [67], which performs batch PIR with simple bucketing. This approach, which is generally more communication efficient

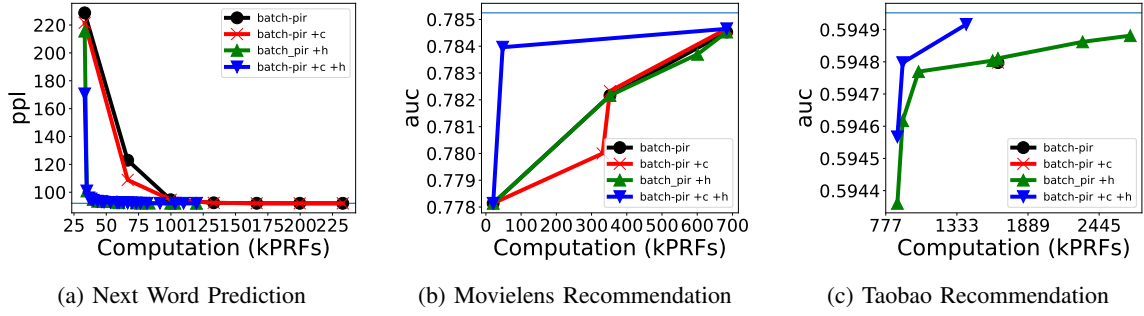


Fig. 12: Pareto curve of tradeoff between computation and accuracy with communication fixed at less than 300KB per inference. Ppl: lower is better; auc: higher is better. The full precision baseline model quality is shown as teal line.

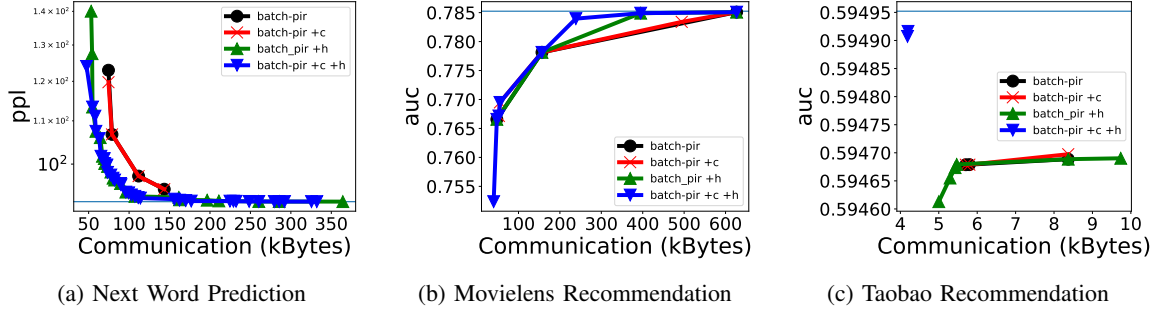


Fig. 13: Pareto curve of tradeoff between communication and accuracy wwith computation fixed at less than 100K PRFs (with exception of Taobao, where computation is fixed at less3 than 5M PRFs). Ppl: lower is better; auc: higher is better. The full precision baseline model quality is shown as teal line.

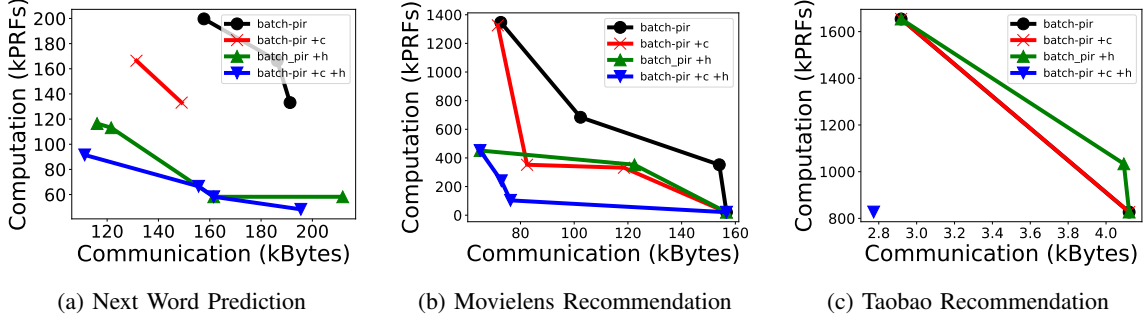


Fig. 14: Pareto curve of tradeoff between communication with model accuracy fixed to be within 2% of the baseline.

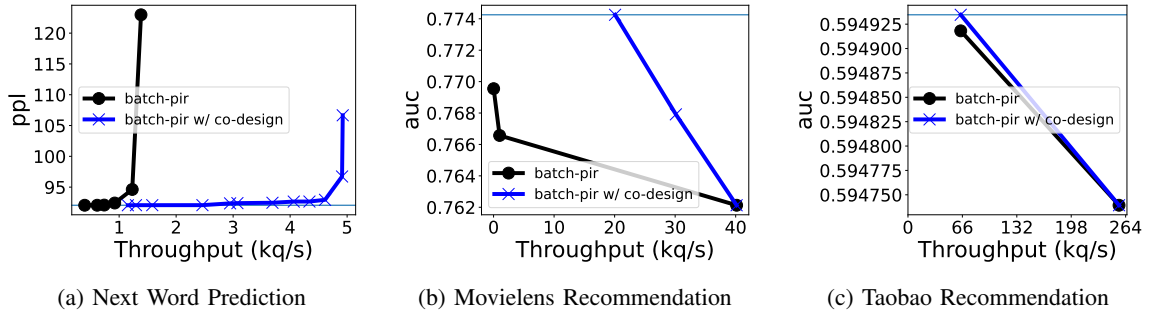


Fig. 15: System throughput vs model quality with and without co-design across applications on a single V100 GPU. Communication is fixed to be < 300KB per inference, and latency to be < 100ms. Ppl: lower is better; auc: higher is better. 1 kq/s = 1,000 queries per second.

than the ones proposed previously, comes at an expense: queries may be dropped if they fall in the same bucket. We show that the noise tolerance of ML allows the use of such probabilistic PIR protocols, and the careful co-design of batch

PIR and ML can make this simple batch PIR practical with minimal accuracy loss.

**On-device ML** On-device ML has garnered significant attention in recent years and span applications including recommendation [39], [44], speech recognition [1], translation [71], etc. Our work considers on-device ML for privacy, and enables the use of large server-side embedding tables for on-device inference.

## VII. CONCLUSION

We present a system for efficiently and privately serving embeddings for on-device ML applications. Our main contribution is a system that employs: 1) efficient GPU acceleration for DPF-based PIR schemes, and 2) co-design of ML with batch PIR. Together, on various on-device ML applications including recommendation and language modeling, our system on a single V100 GPU can serve up to 100,000 queries per second—a  $> 100\times$  speedup over a naively implemented system on a multi-core CPU—while maintaining model accuracy, and limiting communication to be within 300KB and response latency to  $< 100\text{ms}$ , respectively.

## REFERENCES

- [1] “Amazon on device speech recognition,” <https://www.amazon.science/blog/how-to-make-on-device-speech-recognition-practical>.
- [2] “Amd sev,” <https://developer.amd.com/sev/>.
- [3] “Apple app tracking transparency,” <https://developer.apple.com/documentation/apptestingtransparency>.
- [4] “Apple privacy changes hammer social media stocks beyond meta,” <https://news.yahoo.com/apple-privacy-changes-hammer-social-media-stocks-beyond-meta-162759059.html>.
- [5] “Arm trustzone,” <https://www.arm.com/technologies/trustzone-for-cortex-a>.
- [6] “Ccpa,” <https://www.oag.ca.gov/privacy/ccpa>.
- [7] “Chacha stream cipher in tls,” <https://www.rfc-editor.org/rfc/rfc7905>.
- [8] “Deep learning recommendation model,” <https://www.adityaagrawal.net/blog/dnn/dlrm>.
- [9] “Gdpr,” <https://gdpr.eu/what-is-gdpr/>.
- [10] “Google cross to restrict cross app tracking,” <https://www.pcmag.com/news/google-to-restrict-cross-app-tracking-of-users-on-android>.
- [11] “Google on device ml,” <https://developers.google.com/learn/topics/on-device-ml/learn-more>.
- [12] “Google research distributed point function,” [https://github.com/google/distributed\\_point\\_functions](https://github.com/google/distributed_point_functions).
- [13] “Intel sgx,” <https://www.intel.com/content/www/us/en/developer/tools/software-guard-extensions/overview.html>.
- [14] “Nvidia cooperative groups,” <https://developer.nvidia.com/blog/cooperative-groups/>.
- [15] “Taobao ad dataset,” <https://www.kaggle.com/datasets/pavansanagapati/ad-displayclick-data-on-taobaocom>.
- [16] “Zipf’s law,” [https://en.wikipedia.org/wiki/Zipf%27s\\_law](https://en.wikipedia.org/wiki/Zipf%27s_law).
- [17] J. Alakuijala, B. Cox, and J. Wassenberg, “Fast keyed hash/pseudo-random function using simd multiply and permute,” 2016. [Online]. Available: <https://arxiv.org/abs/1612.06257>
- [18] S. Angel, H. Chen, K. Laine, and S. Setty, “Pir with compressed queries and amortized query processing,” in *2018 IEEE Symposium on Security and Privacy (SP)*, 2018, pp. 962–979.
- [19] S. Angel, H. Chen, K. Laine, and S. Setty, “Pir with compressed queries and amortized query processing,” in *2018 IEEE Symposium on Security and Privacy (SP)*, 2018, pp. 962–979.
- [20] J.-P. Aumasson and D. J. Bernstein, “Siphash: A fast short-input prf,” in *Progress in Cryptology - INDOCRYPT 2012*, S. Galbraith and M. Nandi, Eds. Berlin, Heidelberg: Springer Berlin Heidelberg, 2012, pp. 489–508.
- [21] J.-P. Aumasson, S. Fischer, S. Khazaei, W. Meier, and C. Rechberger, “New features of latin dances: Analysis of salsa, chacha, and rumba,” in *Fast Software Encryption*, K. Nyberg, Ed. Berlin, Heidelberg: Springer Berlin Heidelberg, 2008, pp. 470–488.
- [22] D. J. Bernstein, *The Salsa20 Family of Stream Ciphers*. Berlin, Heidelberg: Springer Berlin Heidelberg, 2008, pp. 84–97. [Online]. Available: [https://doi.org/10.1007/978-3-540-68351-3\\_8](https://doi.org/10.1007/978-3-540-68351-3_8)
- [23] P. Bojanowski, E. Grave, A. Joulin, and T. Mikolov, “Enriching word vectors with subword information,” *arXiv preprint arXiv:1607.04606*, 2016.
- [24] E. Boyle, N. Gilboa, and Y. Ishai, “Function secret sharing,” 04 2015, pp. 337–367.
- [25] E. Boyle, N. Gilboa, and Y. Ishai, “Secure computation with preprocessing via function secret sharing,” *Cryptology ePrint Archive*, Paper 2019/1095, 2019, <https://eprint.iacr.org/2019/1095>. [Online]. Available: <https://eprint.iacr.org/2019/1095>
- [26] D. Cao, M. Zhang, H. Lu, X. Ye, D. Fan, Y. Che, and R. Wang, “Stream-line ring oram accesses through spatial and temporal optimization,” in *2021 IEEE International Symposium on High-Performance Computer Architecture (HPCA)*, 2021, pp. 14–25.
- [27] B. Chor, E. Kushilevitz, O. Goldreich, and M. Sudan, “Private information retrieval,” *J. ACM*, vol. 45, no. 6, p. 965–981, nov 1998. [Online]. Available: <https://doi.org/10.1145/293347.293350>
- [28] H. Corrigan-Gibbs, D. Boneh, and D. Mazières, “Riposte: An anonymous messaging system handling millions of users,” in *2015 IEEE Symposium on Security and Privacy*, 2015, pp. 321–338.
- [29] H. Corrigan-Gibbs, A. Henzinger, and D. Kogan, “Single-server private information retrieval with sublinear amortized time,” in *Advances in Cryptology - EUROCRYPT 2022 - 41st Annual International Conference on the Theory and Applications of Cryptographic Techniques, Trondheim, Norway, May 30 - June 3, 2022, Proceedings, Part II*, ser. Lecture Notes in Computer Science, O. Dunkelman and S. Dziembowski, Eds., vol. 13276. Springer, 2022, pp. 3–33. [Online]. Available: [https://doi.org/10.1007/978-3-031-07085-3\\_1](https://doi.org/10.1007/978-3-031-07085-3_1)
- [30] I. Dagan, F. Pereira, and L. Lee, “Similarity-based estimation of word cooccurrence probabilities,” in *Proceedings of the 32nd Annual Meeting on Association for Computational Linguistics*, ser. ACL ’94. USA: Association for Computational Linguistics, 1994, p. 272–278. [Online]. Available: <https://doi.org/10.3115/981732.981770>
- [31] J. Doerner and A. Shelat, “Scaling oram for secure computation,” in *Proceedings of the 2017 ACM SIGSAC Conference on Computer and Communications Security*, ser. CCS ’17. New York, NY, USA: Association for Computing Machinery, 2017, p. 523–535. [Online]. Available: <https://doi.org/10.1145/3133956.3133967>
- [32] P. Dufer, M. Zhao, M. Schmitt, A. Fraser, and H. Schütze, “Embedding learning through multilingual concept induction,” 2018. [Online]. Available: <https://arxiv.org/abs/1801.06807>
- [33] C. W. Fletcher, L. Ren, A. Kwon, M. Van Dijk, and S. Devadas, “Free recursive oram: [nearly] free recursion and integrity verification for position-based oblivious ram,” in *Proceedings of the Twentieth International Conference on Architectural Support for Programming Languages and Operating Systems*, 2015, pp. 103–116.
- [34] C. Gentry, “Fully homomorphic encryption using ideal lattices,” in *Proceedings of the Forty-First Annual ACM Symposium on Theory of Computing*, ser. STOC ’09. New York, NY, USA: Association for Computing Machinery, 2009, p. 169–178. [Online]. Available: <https://doi.org/10.1145/1536414.1536440>
- [35] C. Gentry and S. Halevi, “Compressible fhe with applications to pir,” *IACR Cryptol. ePrint Arch.*, vol. 2019, p. 733, 2019.
- [36] N. Gilboa and Y. Ishai, “Distributed point functions and their applications,” in *EUROCRYPT*, 2014.
- [37] O. Goldreich, S. Goldwasser, and S. Micali, “How to construct random functions,” *J. ACM*, vol. 33, no. 4, p. 792–807, aug 1986. [Online]. Available: <https://doi.org/10.1145/6490.6503>
- [38] O. Goldreich and R. Ostrovsky, “Software protection and simulation on oblivious rams,” *J. ACM*, vol. 43, no. 3, p. 431–473, may 1996. [Online]. Available: <https://doi.org/10.1145/233551.233553>
- [39] Y. Gong, Z. Jiang, Y. Feng, B. Hu, K. Zhao, Q. Liu, and W. Ou, “Edgerec: Recommender system on edge in mobile taobao,” 10 2020, pp. 2477–2484.
- [40] H. Gupta, S. Hsia, V. Saraph, X. Wang, B. Reagen, G.-Y. Wei, H.-H. S. Lee, D. Brooks, and C.-J. Wu, “Deeprecsys: A system for optimizing end-to-end at-scale neural recommendation inference,” in

- [41] U. Gupta, C. Wu, X. Wang, M. Naumov, B. Reagen, D. Brooks, B. Cottel, K. M. Hazelwood, M. Hempstead, B. Jia, H. S. Lee, A. Malevich, D. Mudigere, M. Smelyanskiy, L. Xiong, and X. Zhang, “The architectural implications of facebook’s dnn-based personalized recommendation,” in *IEEE International Symposium on High Performance Computer Architecture, HPCA 2020, San Diego, CA, USA, February 22–26, 2020*. IEEE, 2020, pp. 488–501. [Online]. Available: <https://doi.org/10.1109/HPCA47549.2020.00047>
- [42] H. Handschuh, *SHA Family (Secure Hash Algorithm)*. Boston, MA: Springer US, 2005, pp. 565–567. [Online]. Available: [https://doi.org/10.1007/0-387-23483-7\\_388](https://doi.org/10.1007/0-387-23483-7_388)
- [43] F. M. Harper and J. A. Konstan, “The movielens datasets: History and context,” *ACM Trans. Interact. Intell. Syst.*, vol. 5, no. 4, dec 2015. [Online]. Available: <https://doi.org/10.1145/2827872>
- [44] M. Hejaziinia, D. Huba, I. Leontiadis, K. Maeng, M. Malek, L. Melis, I. Mironov, M. Nasr, K. Wang, and C.-J. Wu, “Fel: High capacity learning for recommendation and ranking via federated ensemble learning,” 2022. [Online]. Available: <https://arxiv.org/abs/2206.03852>
- [45] R. Henry, “Polynomial batch codes for efficient it-pir,” *Proceedings on Privacy Enhancing Technologies*, vol. 2016, 02 2016.
- [46] W. Hua, M. Umar, Z. Zhang, and G. E. Suh, “Guardnn: Secure accelerator architecture for privacy-preserving deep learning,” in *Proceedings of the 59th ACM/IEEE Design Automation Conference*, ser. DAC ’22. New York, NY, USA: Association for Computing Machinery, 2022, p. 349–354. [Online]. Available: <https://doi.org/10.1145/3489517.3530439>
- [47] W. Hua, M. Umar, Z. Zhang, and G. E. Suh, “Mgx: Near-zero overhead memory protection for data-intensive accelerators,” in *Proceedings of the 49th Annual International Symposium on Computer Architecture*, ser. ISCA ’22. New York, NY, USA: Association for Computing Machinery, 2022, p. 726–741. [Online]. Available: <https://doi.org/10.1145/3470496.3527418>
- [48] Y. Ishai, E. Kushilevitz, R. Ostrovsky, and A. Sahai, “Batch codes and their applications,” in *Proceedings of the Thirty-Sixth Annual ACM Symposium on Theory of Computing*, ser. STOC ’04. New York, NY, USA: Association for Computing Machinery, 2004, p. 262–271. [Online]. Available: <https://doi.org/10.1145/1007352.1007396>
- [49] C. Juvekar, V. Vaikuntanathan, and A. Chandrakasan, “GAZELLE: A low latency framework for secure neural network inference,” in *27th USENIX Security Symposium (USENIX Security 18)*. Baltimore, MD: USENIX Association, Aug. 2018, pp. 1651–1669. [Online]. Available: <https://www.usenix.org/conference/usenixsecurity18/presentation/juvekar>
- [50] Y. Kang, J. Hauswald, C. Gao, A. Rovinski, T. Mudge, J. Mars, and L. Tang, “Neurosurgeon: Collaborative intelligence between the cloud and mobile edge,” *SIGARCH Comput. Archit. News*, vol. 45, no. 1, p. 615–629, apr 2017. [Online]. Available: <https://doi.org/10.1145/3093337.3037698>
- [51] B. Knott, S. Venkataraman, A. Y. Hannun, S. Sengupta, M. Ibrahim, and L. van der Maaten, “Crypten: Secure multi-party computation meets machine learning,” in *Neural Information Processing Systems*, 2021.
- [52] V. I. Kolobov, E. Boyle, N. Gilboa, and Y. Ishai, “Programmable distributed point functions,” Springer-Verlag, 2022.
- [53] N. Kumar, M. Rathee, N. Chandran, D. Gupta, A. Rastogi, and R. Sharma, “Cryptflow: Secure tensorflow inference,” in *IEEE Symposium on Security and Privacy*. IEEE, May 2020. [Online]. Available: <https://www.microsoft.com/en-us/research/publication/cryptflow-secure-tensorflow-inference/>
- [54] Y. Lee, S. H. Seo, H. Choi, H. U. Sul, S. Kim, J. W. Lee, and T. J. Ham, “Merci: Efficient embedding reduction on commodity hardware via sub-query memoization,” in *Proceedings of the 26th ACM International Conference on Architectural Support for Programming Languages and Operating Systems*, ser. ASPLOS ’21. New York, NY, USA: Association for Computing Machinery, 2021, p. 302–313. [Online]. Available: <https://doi.org/10.1145/3445814.3446717>
- [55] G. Liu, K. Li, Z. Xiao, and R. Wang, “Ps-oram: Efficient crash consistency support for oblivious ram on nvme,” in *Proceedings of the 49th Annual International Symposium on Computer Architecture*, ser. ISCA ’22. New York, NY, USA: Association for Computing Machinery, 2022, p. 188–203. [Online]. Available: <https://doi.org/10.1145/3470496.3527425>
- [56] S. J. Menon and D. J. Wu, “Spiral: Fast, high-rate single-server pir via fhe composition,” *Cryptology ePrint Archive*, Paper 2022/368, 2022, <https://eprint.iacr.org/2022/368>. [Online]. Available: <https://eprint.iacr.org/2022/368>
- [57] S. Merity, C. Xiong, J. Bradbury, and R. Socher, “Pointer sentinel mixture models,” 2016. [Online]. Available: <https://arxiv.org/abs/1609.07843>
- [58] T. Mikolov, K. Chen, G. S. Corrado, and J. Dean, “Efficient estimation of word representations in vector space,” 2013. [Online]. Available: <http://arxiv.org/abs/1301.3781>
- [59] P. Mishra, R. Lehmkuhl, A. Srinivasan, W. Zheng, and R. A. Popa, “Delphi: A cryptographic inference service for neural networks,” in *29th USENIX Security Symposium (USENIX Security 20)*. USENIX Association, Aug. 2020, pp. 2505–2522. [Online]. Available: <https://www.usenix.org/conference/usenixsecurity20/presentation/mishra>
- [60] D. Mudigere, Y. Hao, J. Huang, Z. Jia, A. Tulloch, S. Sridharan, X. Liu, M. Ozdal, J. Nie, J. Park, L. Luo, J. A. Yang, L. Gao, D. Ivchenko, A. Basant, Y. Hu, J. Yang, E. K. Ardestani, X. Wang, R. Komuravelli, C.-H. Chu, S. Yilmaz, H. Li, J. Qian, Z. Feng, Y. Ma, J. Yang, E. Wen, H. Li, L. Yang, C. Sun, W. Zhao, D. Melts, K. Dhulipala, K. Kishore, T. Graf, A. Eisenman, K. K. Matam, A. Gangidi, G. J. Chen, M. Krishnan, A. Nayak, K. Nair, B. Muthiah, M. Khorashadi, P. Bhattacharya, P. Lapukhov, M. Naumov, A. Mathews, L. Qiao, M. Smelyanskiy, B. Jia, and V. Rao, “Software-hardware co-design for fast and scalable training of deep learning recommendation models,” in *Proceedings of the 49th Annual International Symposium on Computer Architecture*, ser. ISCA ’22. New York, NY, USA: Association for Computing Machinery, 2022, p. 993–1011. [Online]. Available: <https://doi.org/10.1145/3470496.3533727>
- [61] M. Naumov, D. Mudigere, H. M. Shi, J. Huang, N. Sundaraman, J. Park, X. Wang, U. Gupta, C. Wu, A. G. Azzolini, D. Dzhuigakov, A. Mallevich, I. Cherniavskii, Y. Lu, R. Krishnamoorthi, A. Yu, V. Kondratenko, S. Pereira, X. Chen, W. Chen, V. Rao, B. Jia, L. Xiong, and M. Smelyanskiy, “Deep learning recommendation model for personalization and recommendation systems,” *CoRR*, vol. abs/1906.00091, 2019. [Online]. Available: <https://arxiv.org/abs/1906.00091>
- [62] NLLB Team, M. R. Costa-jussà, J. Cross, O. Çelebi, M. Elbayad, K. Heffernan, E. Kalbassi, J. Lam, D. Licht, J. Maillard, A. Sun, S. Wang, G. Wenzek, A. Youngblood, B. Akula, L. Barrault, G. M. Gonzalez, P. Hansanti, J. Hoffman, S. Jarrett, K. R. Sadagopan, D. Rowe, S. Spruit, C. Tran, P. Andrews, N. F. Ayan, S. Bhosale, S. Edunov, A. Fan, C. Gao, V. Goswami, F. Guzmán, P. Koehn, A. Mourachko, C. Ropers, S. Saleem, H. Schwenk, and J. Wang, “No language left behind: Scaling human-centered machine translation,” 2022. [Online]. Available: <https://arxiv.org/abs/2207.04672>
- [63] J. Pennington, R. Socher, and C. Manning, “Glove: Global vectors for word representation,” vol. 14, 01 2014, pp. 1532–1543.
- [64] R. Rajat, Y. Wang, and M. Annamalai, “Laoram: A look ahead oram architecture for training large embedding tables,” 2021.
- [65] M. Raoufi, Y. Zhang, and J. Yang, “Ir-oram: Path access type based memory intensity reduction for path-oram,” in *2022 IEEE International Symposium on High-Performance Computer Architecture (HPCA)*, 2022, pp. 360–372.
- [66] L. Ren, X. Yu, C. W. Fletcher, M. Van Dijk, and S. Devadas, “Design space exploration and optimization of path oblivious ram in secure processors,” in *Proceedings of the 40th Annual International Symposium on Computer Architecture*, 2013, pp. 571–582.
- [67] S. Servan-Schreiber, S. Langowski, and S. Devadas, “Private approximate nearest neighbor search with sublinear communication,” in *2022 IEEE Symposium on Security and Privacy (SP)*, 2022, pp. 911–929.
- [68] A. Shamir, “How to share a secret,” *Commun. ACM*, vol. 22, no. 11, p. 612–613, nov 1979. [Online]. Available: <https://doi.org/10.1145/359168.359176>
- [69] E. Stefanov, M. V. Dijk, E. Shi, T.-H. H. Chan, C. Fletcher, L. Ren, X. Yu, and S. Devadas, “Path oram: An extremely simple oblivious ram protocol,” *J. ACM*, vol. 65, no. 4, apr 2018. [Online]. Available: <https://doi.org/10.1145/3177872>
- [70] G. E. Suh, D. Clarke, B. Gassend, M. van Dijk, and S. Devadas, “Aegis: Architecture for tamper-evident and tamper-resistant processing,” in *Proceedings of the 17th Annual International Conference on Supercomputing*, ser. ICS ’03. New York, NY, USA: Association for Computing Machinery, 2003, p. 160–171. [Online]. Available: <https://doi.org/10.1145/782814.782838>



- [71] Z. Tan, Z. Yang, M. Zhang, Q. Liu, M. Sun, and Y. Liu, "Dynamic multi-branch layers for on-device neural machine translation," *IEEE/ACM Transactions on Audio, Speech, and Language Processing*, vol. 30, pp. 958–967, 2022. [Online]. Available: <https://doi.org/10.1109%2Ftaslp.2022.3153257>
- [72] S. Wagh, S. Tople, F. Benhamouda, E. Kushilevitz, P. Mittal, and T. Rabin, "Falcon: Honest-majority maliciously secure framework for private deep learning," 2020. [Online]. Available: <https://arxiv.org/abs/2004.02229>
- [73] R. Wang, Y. Zhang, and J. Yang, "Cooperative path-oram for effective memory bandwidth sharing in server settings," in *2017 IEEE International Symposium on High Performance Computer Architecture (HPCA)*. IEEE, 2017, pp. 325–336.
- [74] R. Wang, Y. Zhang, and J. Yang, "D-oram: Path-oram delegation for low execution interference on cloud servers with untrusted memory," in *2018 IEEE International Symposium on High Performance Computer Architecture (HPCA)*. IEEE, 2018, pp. 416–427.
- [75] X. Wang, H. Chan, and E. Shi, "Circuit oram: On tightness of the goldreich-ostrovsky lower bound," in *Proceedings of the 22nd ACM SIGSAC Conference on Computer and Communications Security*, 2015, pp. 850–861.
- [76] X. Xia, H. Yin, J. Yu, Q. Wang, G. Xu, and Q. V. H. Nguyen, "On-device next-item recommendation with self-supervised knowledge distillation," in *Proceedings of the 45th International ACM SIGIR Conference on Research and Development in Information Retrieval*, ser. SIGIR '22. New York, NY, USA: Association for Computing Machinery, 2022, p. 546–555. [Online]. Available: <https://doi.org/10.1145/3477495.3531775>
- [77] G. Zhou, X. Zhu, C. Song, Y. Fan, H. Zhu, X. Ma, Y. Yan, J. Jin, H. Li, and K. Gai, "Deep interest network for click-through rate prediction," in *Proceedings of the 24th ACM SIGKDD International Conference on Knowledge Discovery Data Mining*, ser. KDD '18. New York, NY, USA: Association for Computing Machinery, 2018, p. 1059–1068. [Online]. Available: <https://doi.org/10.1145/3219819.3219823>